2026 IEEE/SICE International Symposium on System Integration (SII)
January 11-14, 2026. Cancún, México

Wire-Driven Reconfigurable Soft Modular Robot for Multi-Modal Locomotion

Sakura Yamaguchi[1] and Ryuma Niiyama[1]

***Abstract*— Soft locomotion robots, leveraging compliant materials, adapt well to complex terrains, yet research evaluating variations in body configuration and achieving multiple locomotion modes within a single system remains limited. We present a reconfigurable soft modular robot combining urethane chip foam flexibility with modular versatility. Wire-driven actuation enables controllable deformation, allowing even a single module to move via passive body dynamics. The modular design supports rapid reconfiguration into serial connections, as well as lateral connections in either midpoint-connected (H-shape) or end-connected (V-shape) layouts. Experiments under simplified CPG-inspired oscillatory control assessed locomotion performance and terrain adaptability. The V-shape reached 34.70 mm/s, while the serial configuration with bottom-contact excelled in climbing 10 mm steps and traversing artificial grass. Adjusting actuation intervals improved deformation retention and propulsion. These results show that combining flexibility and reconfigurability enables diverse locomotion modes and robust environmental adaptability.**

I. INTRODUCTION

Modular configurations are an effective strategy for enhancing the reconfigurability and scalability of robotic systems. In hard modular robotics, rigid modules have enabled diverse designs that exploit self-reconfiguration, redundancy, and structural flexibility [3][6]. Such modularity also benefits locomotion robots by allowing configuration changes to match terrain or task, improving robustness through damage recovery, and adapting locomotion strategies to different layouts. Soft robotics, by contrast, enables large deformations (e.g., bending, compression, twisting) through compliant structures. These properties enable high contact safety and terrain adaptability, making soft robots promising for locomotion in complex environments [5][11]. SMA actuators provide high energy density, a large power-to-weight ratio, and a compact form, making them widely used in soft and bio-inspired robots[5][7].However, they face common limitations—slow cooling, low recoverable strain, and nonlinear hysteresis—which restrict operating frequency and make continuous or fast-cycling locomotion difficult. Pneumatic actuators, on the other hand, enable large deformations and high power output, yet they require external compressors and tubing to regulate airflow, which constrains modularity and tether-free deployment [9] [13]. In contrast, wire-driven actuation provides a lightweight and electrically controllable alternative that simplifies modular integration. By embedding compact motors and routing tendons through flexible bodies, this approach provides high controllability and output while preserving mechanical simplicity. In addition, because power and control can be supplied electrically, wire-driven soft modules are comparatively well suited for future realization of fully untethered, battery-powered systems, offering a more feasible path toward reconfigurable and scalable locomotion robots than other actuation methods.

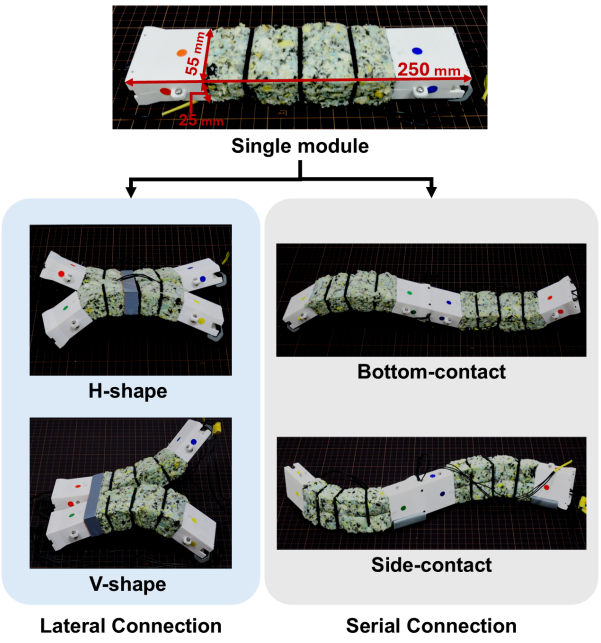

Fig. 1: The reconfigurable soft modular robot proposed in this paper. The fundamental single module is at the top. Below are two types of lateral connections (H-shape and V-shape) and two serial configurations (bottom-contact and side-contact).

Despite these advantages, few systems have unified the flexibility of soft bodies with the configurational versatility of modular designs. Previous studies on soft modules have often restricted connectivity to serial layouts [13], fixed the structure without reconfiguration [12], or limited reconfiguration to radial arrangements [8]. While modularized soft quadrupeds have improved manufacturing efficiency [1], they have not explored diverse configurations or locomotion variability.

We present a wire-driven soft modular robot that can be flexibly reconfigured into serial and lateral layouts (single, serial, H, V; Fig. 1). This study contributes by developing a compliant modular structure and demonstrating that combining structural reconfiguration with simple CPG-like control

[1]Graduate School of Science and Technology, Mechanical Engineering, Meiji University, 1-1-1 Higashi-Mita, Tama-ku, Kawasaki-shi, Kanagawa, Japan

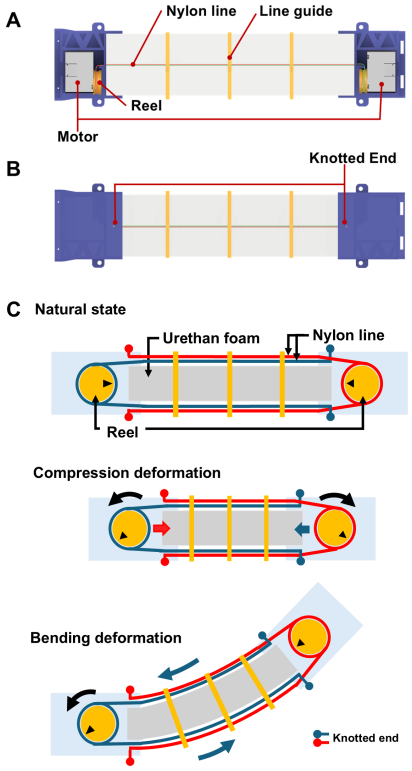

Fig. 2: Basic configuration of the wire-driven soft modular robot. The central urethane foam segment is connected to motors mounted at both ends via nylon lines. (c) Schematic showing how motor rotation winds the line, causing compression and bending of the urethane foam.

enables versatile and adaptable motion generation.

II. METHOD

A. Design Concept

The design concept is to leverage the inherent flexibility of soft materials—particularly bending and stretching deformations—while combining the structural advantages of modular robots with the characteristics of soft robots. By reconfiguring the modular structure, we aim to achieve diverse locomotion modes and high environmental adaptability. The robot uses a wire-driven actuation method, where motors pull wires to induce deformation. This approach offers the advantage of high controllability and output while maintaining structural flexibility[2]. This method is widely adopted in soft robotics, as seen in studies of caterpillar-inspired robots for iterative motor learning[10] and switching-legged robots that actively control ground contact[4].

Building on this concept, we designed a fundamental module that forms the basis for all configurations described in the next section.

B. Fundamental Module Structure

The proposed robot is a modular soft robot equipped with two motors (ROBOTIS, DYNAMIXEL XC330-T288) mounted at both ends. Its primary deformation mechanism is

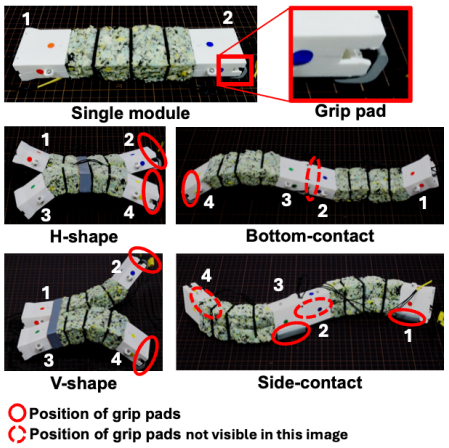

Fig. 3: Configuration of grip pads and motor arrangement. Red ellipses indicate the positions of the grip pads. Numbers 1–4 represent motor IDs. In the CPG control, the specified phase difference (e.g., 90°) is applied sequentially between adjacent motors (1–2, 2–3, and 3–4).

based on pulling a sponge-like flexible structure using wires, as illustrated in Fig.2. The flexible part is made of urethane chip foam. The flexible part is made of urethane chip foam, a material that is more resistant to permanent deformation than ordinary urethane while retaining softness and elasticity.

Each module incorporates a wire guide that stabilizes the wire path, thereby preventing unintended friction and deformation. The control computer, power supply, and the U2D2 USB serial interface for two-way communication with the DYNAMIXEL motors are located externally and are not mounted on the robot. Each nylon wire was tied without slack so that, when the robot body was manually bent by holding both ends, the rotational section of the motor housing rotated accordingly—confirming proper connection and appropriate initial tension.

The motor housings, fabricated from PLA, enclose the motors. A 4mm-thick highly elastic NBR corner grip pad is attached with double-sided tape as an anti-slip feature. The position of this grip pad can be changed to match the robot's configuration. In the basic configuration (Fig. 1 Single module), the grip pad is attached to only one end, creating directional (anisotropic) friction. This design is inspired by the two-anchor crawling locomotion found in biology, where organisms use differential friction to move forward. While living organisms use setae or mucus for this, our study uses a simple implementation by differentiating the presence or absence of the grip pad.

For serial configurations, modules connect via coupling components integrated into the motor housings, while for lateral configurations, external connectors can be attached.

C. Module Configurations

We propose four configurations composed of two modules. In the serial configuration, multiple modules are connected end-to-end to create a longer structure, enabling wave-like body motions. For lateral connections, modules can be

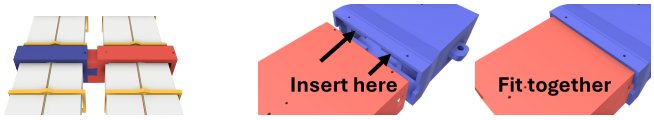

(a) (b)

Fig. 4: Connector designs for lateral and serial configurations. (a) Lateral connection using detachable PLA connectors attached post-fabrication. The connectors use a snap-fit design and are secured by friction. (b) Serial connection by inserting and aligning motor housing ends. One module end is inserted into the other and then fastened with screws.

connected in two ways: at their central soft material segments to form an H-shape configuration, or at their ends near the motor housings to form a V-shape configuration.

The proposed modular robot is designed for flexible reconfiguration into various structures. The methods for connecting modules are straightforward. For lateral connections, PLA connectors are attached to clamp onto either the midpoint or the motor-side end of each module after fabrication. These connectors use a snap-fit design and are secured by friction, as shown in Fig. 4(a). For serial connections, the motor housing end of one module is inserted into the coupling slot of another and then fastened with screws, which ensures a secure and aligned connection (Fig. 4(b)).

D. Control Method

The proposed robot utilizes a wire-driven mechanism in which sponge-based soft components are deformed by multiple motors pulling tendons. To coordinate these motors, we adopt a phase-synchronization control scheme based on coupled oscillators. While inspired by biological Central Pattern Generators (CPGs), this approach differs from neuron-based CPGs in that it is implemented as a simplified engineering model using periodic functions.

Specifically, the phase ϕ_i of a virtual oscillator corresponding to each motor is updated according to the following equations, with a corrective term introduced to maintain a phase difference γ between adjacent oscillators:

$$\dot{\phi}_i = \omega + K_c(\phi_{neighbor} - \phi_i - \gamma) \quad (1)$$

Here, ω denotes the b ase angular velocity, and K_c is a coupling strength coefficient. When the phase difference between oscillators deviates from the target, the system applies mutual corrections to converge toward synchronized oscillations across all motors.

Each motor was actuated in a feedforward manner by transmitting target positions generated from sinusoidal functions of ϕ via the Dynamixel SDK, with fixed phase relationships explicitly defined in the command signals and not dynamically varied. Control parameters are summarized in Table I.

In preliminary tests conducted under the same conditions as the main experiments, it was observed that $\omega = 6$ rad/s provided a good balance between maintaining oscillation amplitude and maximizing propulsive force from deformation. Higher angular velocities reduced amplitude due to inertial effects, while lower values reduced deformation speed, both of which hindered propulsion.

TABLE I: The control parameters used in this study

Parameter	Value
Amplitude of sine wave (motion range)	4000
Phase difference between motors γ	90°, 180°, 270°
Angular velocity ω	6.0 rad/s
Correction coefficient for phase error K_c	0.5

III. EXPERIMENT

In this section, we evaluate the locomotion performance of each module configuration based on movement speed on a flat surface and, for selected cases, the ability to traverse obstacle environments such as steps. The experiments were conducted on a soft PVC cutter mat, and the step height was set to 10 mm.

To evaluate locomotion performance, comparative experiments were conducted with phase differences between motors set to 90°,180°, and 270°. However, only for the side-contact configuration, a comparison of performance was made by varying the angular velocity instead of the phase difference, as this was deemed a more suitable evaluation for its locomotion mode.

The robot exhibits periodic locomotion, and thus the measured speed over a certain travel distance represents an averaged velocity across repeated gait cycles. In all tested patterns, the behavior was highly reproducible; therefore, this paper presents the result of a single trial. Within the range of observations conducted in this study, the locomotion behavior remained consistent under the same conditions, without noticeable variation in speed or direction.

In the experiment, a red sticker was placed on the front and a blue sticker on the rear of the first module, while a green sticker was placed on the front and a yellow sticker on the rear of the second module. These were assigned as IDs 1–4 and tracked using Kinovea. Additionally, to measure the bending section of the flexible material, the central wire guide was also tracked and labeled as ”mid” in the graphs.

A. Single Module Configuration

First, we measured the locomotion performance of a single module. As shown in Fig.5 B-1, locomotion observed at 180° utilized a compress-and-extend pattern: the urethane chip foam was compressed to anchor the rear part using the grip pad, followed by an extension that propelled the robot forward. In contrast, at 90° the module advanced with the non-frictional side facing forward, while at 270° it moved with the frictional side in front. In both cases, the locomotion was achieved by bending deformation of the urethane chip foam, resulting in distinct movement patterns corresponding to the direction of motion.

As shown in Table II, the highest speed was achieved at 90°.

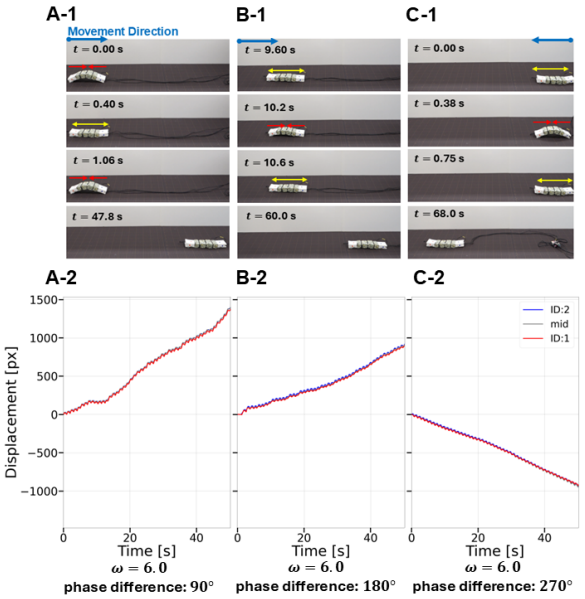

Fig. 5: Locomotion of a single module with phase differences of 90°, 180°, and 270°. Top: motion snapshots (A-1 to C-1); bottom: displacement over time (A-2 to C-2, horizontal axis: time [s], vertical axis: position [px]).

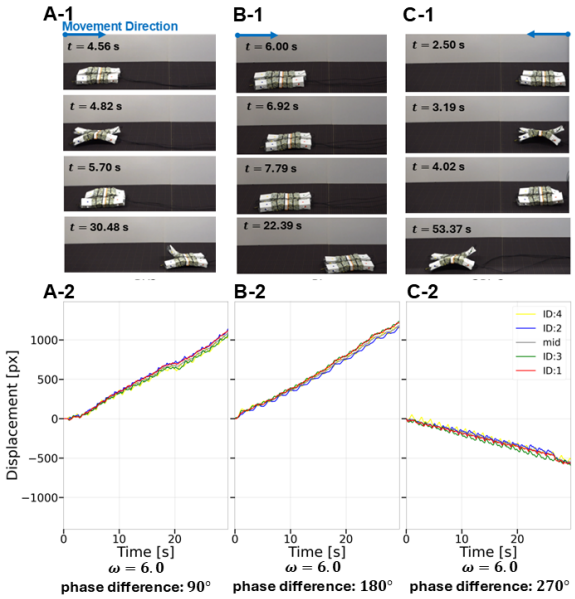

Fig. 6: Locomotion of H-shape configuration with phase differences of 90°, 180°, and 270°. Top: motion snapshots (A-1 to C-1); bottom: displacement over time (A-2 to C-2, horizontal axis: time [s], vertical axis: position [px]).

TABLE II: Locomotion speed of the single module

Phase Difference	Speed
90°	16.75 mm/s
180°	10.29 mm/s
270°	-9.324 mm/s

B. Lateral Connection

1) H-shape configuration: The modules were connected at the center of their soft material sections, resulting in a configuration where the four distal ends functioned like legs. Similar to the single-module configuration, forward locomotion at a phase difference of 180° was achieved through compression and extension, while at 90° and 270°, locomotion was driven by bending deformations. Different locomotion characteristics were observed depending on the configuration. The interaction between modules caused the robot's center of mass to sway during movement, with frequent detachment of the module ends from the ground. The motion of one module influenced the behavior and performance of the other.

In terms of speed, as shown in Fig. 6, the configuration achieved 21.20 mm/s at 90° and 20.92 mm/s at 180°, both exceeding the single-module results, while at 270° the speed was -9.20 mm/s, similar to the single-module case.

2) V-shape configuration: The modules were connected at their motor housing ends to form a V-shaped structure. At 270°, initial attempts failed to produce forward locomotion; however, by reversing the fixed orientation of the module ends, forward movement was achieved. As with the other configurations, the module with the attached grip pad advanced forward.

Across all phase differences, this V-shaped configuration outperformed both the single-module and midpoint-connection configurations. Notably, it achieved a maximum speed of 34.70 mm/s at 180° (Fig. 7, Table III).

TABLE III: Locomotion performance of laterally connected configuration

Connection Type	Phase Difference	Speed
Midpoint	90°	21.20 mm/s
Midpoint	180°	20.92 mm/s
Midpoint	270°	-9.20 mm/s
End	90°	25.24 mm/s
End	180°	34.70 mm/s
End	270°	-23.93 mm/s

C. Serial Connection

Two modules were connected in series along the longitudinal axis, and experiments were conducted for two configurations: bottom-contact and side-contact.

1) Bottom-contact Locomotion: As shown in Table IV and Fig. 8, the configuration achieved results that outperformed the single-module case in all conditions.

TABLE IV: Locomotion performance of serially connected configuration

Contact Surface	Phase Difference	Angular Velocity	Velocity
Bottom	90°	6.0 rad/s	20.68 mm/s
Bottom	180°	6.0 rad/s	16.55 mm/s
Bottom	270°	6.0 rad/s	-18.55 mm/s
Side	90°	4.0 rad/s	20.28 mm/s
Side	90°	6.0 rad/s	11.58 mm/s

2) Side-contact Locomotion: A side-contact configuration was used to investigate locomotion through longitudinal wave-like motion. As shown in Fig.1, grip pads were attached to only one side of the motor housing surface in contact with

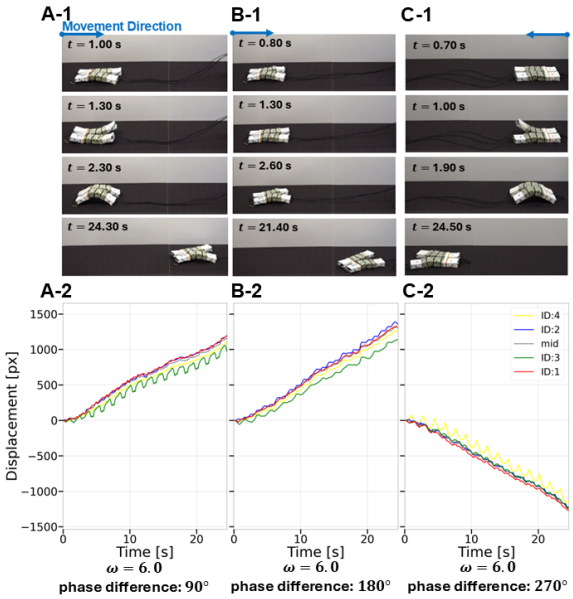

Fig. 7: Locomotion of V-shape configuration with phase differences of 90°, 180°, and 270°. Top: motion snapshots (A-1 to C-1); bottom: displacement over time (A-2 to C-2, horizontal axis: time [s], vertical axis: position [px]).

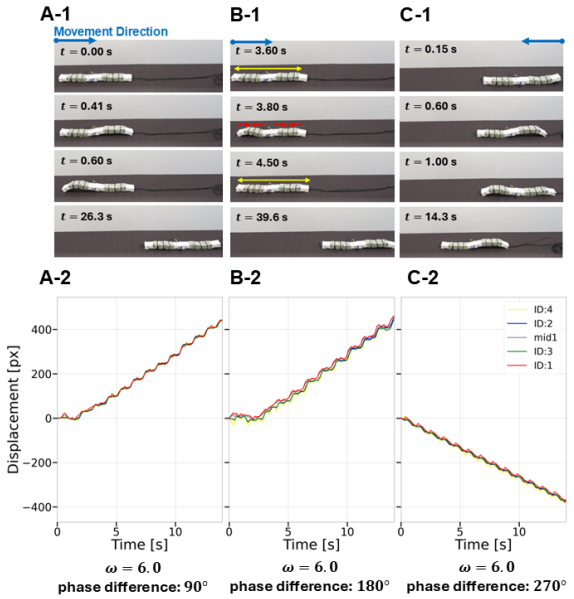

Fig. 8: Locomotion of bottom-contact serial configuration with phase differences of 90°, 180°, and 270°. Top: motion snapshots (A-1 to C-1); bottom: displacement over time (A-2 to C-2, horizontal axis: time [s], vertical axis: position [px]).

the ground and were alternated between adjacent modules. As illustrated in Fig.9 and TableIV, locomotion speed were 20.28 mm/s at 4.0 rad/s and 11.58 mm/s at 6.0 rad/s, suggesting that lower angular velocity may allow more stable and efficient forward motion in longitudinal wave-based locomotion.

D. Terrain Adaptability

The bottom-contact serial configuration was adopted because the rear module maintained stable ground contact, supporting the body during motion. With a phase difference of 90°, the robot exhibited stable locomotion on a 20 mm artificial grass surface (Fig. 10a), demonstrating adaptability to compliant terrain.

In subsequent step-climbing trials, although the motor housing lifted sufficiently, the grip pad failed to reach the top surface of the step, resulting in unsuccessful traversal. To address this issue, we assigned distinct roles to the two modules: the front module is responsible for gripping the step, while the rear module generates propulsion. The motion of the front module was modified by introducing a 1.0 s static interval after its motor actuation, allowing the front could remain lifted and advance far enough to grip the step. With this role division and timing adjustment, the robot achieved the deformation and propulsion necessary to climb a 10 mm step (Fig. 10b).

IV. DISCUSSION

This study demonstrated that the proposed wire-driven soft modular robot can achieve multiple locomotion modes even with a single module. This indicates that the passive deformation of the soft body functions effectively, enabling diverse motions with relatively simple control signals. Reconfiguring the module layout improved both locomotion speed and environmental adaptability.

In lateral configurations, the end-connected (V-shape) type outperformed the center-connected (H-shape) type. In the H-shape, deformation of one module affected the motion of the other, causing instability and fluctuations in the overall center of mass. In contrast, the V-shape exhibited greater freedom of deformation in the central section, while the fixed side maintained stable ground contact due to the weight of two motors. This combination of large deformation, effective momentum transfer, and reduced mutual interference contributed to its higher performance.

In the serial configuration, cooperative front–rear role division enabled step climbing. Asymmetric grip placement also allowed side-contact longitudinal wave locomotion, where performance strongly depended on motor angular velocity. These results show that, despite its simple structure, the robot can change its form to meet task demands for speed, stability, or terrain adaptability—a key advantage over prior designs.

However, limitations remain. Under sine-wave control, continuously varying wire tension sometimes hindered sufficient deformation due to the lack of dwell time after peak actuation. Adding intervals improved performance but required manual tuning. The robot was tethered for power and communication during experiments. The cables were left to hang loosely to avoid any pulling force. During forward motion, when the cable lay in the robot's path, its position was gently adjusted while keeping slack to prevent interference. In backward motion, the tether extended in the opposite direction and did not affect locomotion. While tethering ensured stable operation, it limited autonomy and

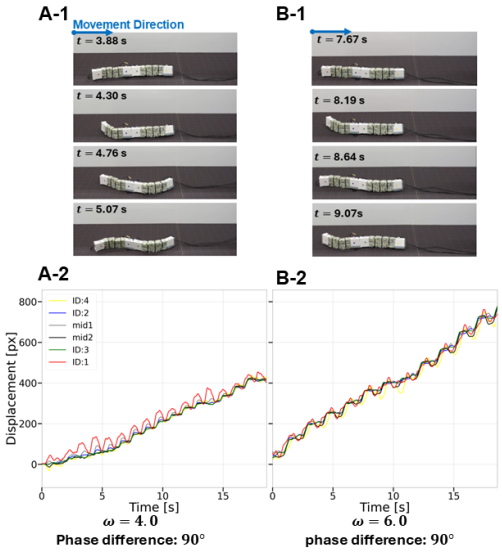

Fig. 9: Locomotion of side-contact serial configuration with phase differences of 90°, 180°, and 270°. Top: motion snapshots (A-1, B-1); bottom: displacement over time (A-2, B-2, horizontal axis: time [s], vertical axis: position [px]).

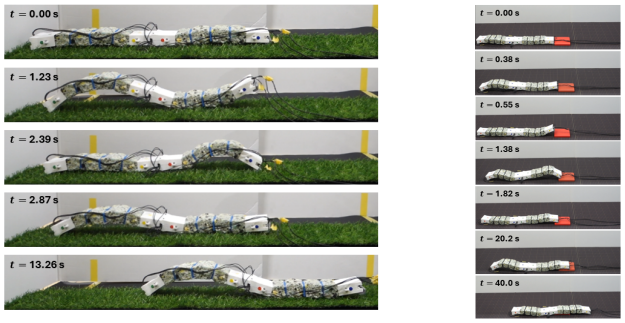

(a) (b)

Fig. 10: Locomotion of the serial configuration robot on uneven surfaces: (a) artificial grass and (b) 1 cm-high step.

mobility. Achieving a fully untethered, stand-alone system with onboard power and control is a key direction for future work, though additional mass and wiring management will pose new challenges. Further studies should also include rigorous baselines against alternative methods, explicit treatment of parameter uncertainty, investigation of dwell-time and initial-tension effects, and long-term tests considering temperature and material viscosity dependencies.

V. CONCLUSION

This study developed a wire-driven soft modular robot that combines the bending and stretching flexibility of soft materials with the structural advantages of modular robots. Experiments demonstrated that reconfiguring the modules enabled distinct locomotion modes, supporting the original design concept. In particular, the serial configuration achieved stable motion on flat and mildly uneven surfaces, such as a single step, and incorporating timing adjustments and role division into the control strategy broadened the range of locomotion behaviors observed. In future work, we aim to develop an untethered version of the robot with onboard power and control and to expand its locomotion capabilities through adaptive, learning-based control for more autonomous operation in diverse environments.

ACKNOWLEDGEMENT

This work was supported by JST Moonshot R&D, Grant Number JPMJMS2013.

REFERENCES

[1] D. D. K. Arachchige, D. M. Perera, S. Mallikarachchi, U. Huzaifa, I. Kanj, and I. S. Godage, "Soft steps: Exploring quadrupedal locomotion with modular soft robots," *IEEE Access*, vol. 11, pp. 63 136–63 148, 2023.

[2] M. Calisti, G. Picardi, and C. Laschi, "Fundamentals of soft robot locomotion," *Journal of The Royal Society Interface*, vol. 14, no. 130, p. 20170101, 2017. [Online]. Available: https://royalsocietypublishing.org/doi/abs/10.1098/rsif.2017.0101

[3] A. Castano, A. Behar, and P. Will, "The conro modules for reconfigurable robots," *IEEE/ASME Transactions on Mechatronics*, vol. 7, no. 4, pp. 403–409, 2002.

[4] X. Chen, P. Stegagno, and C. Yuan, "A cable-driven switching-legged inchworm soft robot: Design and testing," in *2021 American Control Conference (ACC)*, 2021, pp. 2–7.

[5] S. Mao, E. Dong, M. Xu, H. Jin, F. Li, and J. Yang, "Design and development of starfish-like robot: Soft bionic platform with multi-motion using sma actuators," in *2013 IEEE International Conference on Robotics and Biomimetics (ROBIO)*, 2013, pp. 91–96.

[6] S. Murata, E. Yoshida, A. Kamimura, H. Kurokawa, K. Tomita, and S. Kokaji, "M-tran: self-reconfigurable modular robotic system," *IEEE/ASME Transactions on Mechatronics*, vol. 7, no. 4, pp. 431–441, 2002.

[7] R. Niiyama, K. Matsushita, M. Ikeda, K. Or, and Y. Kuniyoshi, "A 3d printed hydrostatic skeleton for an earthworm-inspired soft burrowing robot," *Soft Matter*, vol. 18, pp. 7990–7997, 2022. [Online]. Available: http://dx.doi.org/10.1039/D2SM00882C

[8] C. Schaff, A. Sedal, and M. R. Walter, "Soft robots learn to crawl: Jointly optimizing design and control with sim-to-real transfer," 2022. [Online]. Available: https://arxiv.org/abs/2202.04575

[9] R. F. Shepherd, F. Ilievski, W. Choi, S. A. Morin, A. A. Stokes, A. D. Mazzeo, X. Chen, M. Wang, and G. M. Whitesides, "Multigait soft robot," *Proceedings of the National Academy of Sciences*, vol. 108, no. 51, pp. 20 400–20 403, 2011. [Online]. Available: https://www.pnas.org/doi/abs/10.1073/pnas.1116564108

[10] K. Tezuka and R. Niiyama, "Real-to-real motor learning of tendon-driven soft caterpillar locomotion with world model," in *2024 IEEE 7th International Conference on Soft Robotics (RoboSoft)*, 2024, pp. 579–585.

[11] T. Umedachi, M. Shimizu, and Y. Kawahara, "Caterpillar-inspired crawling robot using both compression and bending deformations," *IEEE Robotics and Automation Letters*, vol. 4, no. 2, pp. 670–676, 2019.

[12] T. Umedachi and B. A. Trimmer, "Autonomous decentralized control for soft-bodied caterpillar-like modular robot exploiting large and continuum deformation," in *2016 IEEE/RSJ International Conference on Intelligent Robots and Systems (IROS)*, 2016, pp. 292–297.

[13] Z. Wan, Y. Sun, Y. Qin, E. H. Skorina, R. Gasoto, M. Luo, J. Fu, and C. D. Onal, "Design, analysis, and real-time simulation of a 3d soft robotic snake," *Soft Robotics*, vol. 10, no. 2, pp. 258–268, 2023, pMID: 35976088. [Online]. Available: https://doi.org/10.1089/soro.2021.0144